Unitarization and low-energy scattering data

P. C. Magalhães* and M. R. Robilotta

Instituto de Física, Universidade de São Paulo, São Paulo, SP, Brazil

(Dated: September 5, 2014)

Abstract

A procedure based on the well known $\mathcal{K}$-matrix formalism is presented, which makes patterns in inelastic regions of low-energy scattering data considerably more transparent. It relies on the use of an empirical kernel, obtained by eliminating elastic loops from the experimental amplitude. This allows structures associated with resonances, such as locations, widths and heights, to become visible with the naked eye. The method is illustrated with a study of the P-wave $K\pi$ amplitude.

arXiv:1404.4111v2 [hep-ph] 4 Sep 2014

*patricia@if.usp.br

I. INTRODUCTION

The problem of understanding the dynamical content of mesonic scattering amplitudes, with energies ranging from threshold to a few GeV, is interesting by itself. Nevertheless, it became especially urgent in recent times, because these amplitudes play important roles in final state interactions which occur after primary weak decays of quarks within D and B mesons. Decays of heavy mesons are presently object of intense scrutiny and the understanding of patterns observed in Dalitz plots require accurate descriptions of both primary weak vertices and hadronic final state interactions[1, 2].

In non-relativistic quantum mechanics, the standard treatment of elastic scattering begins with a potential, which is fed into the Schrödinger equation. In the elastic regime, the potential is real and the dynamical equation yields complex wave-functions, that can be parametrized in terms of phase shifts. When inelasticities are present, one needs a complex optical potential and the corresponding damped wave-functions can be parametrized by their phase shifts and moduli or inelasticity parameters. The formulation of the scattering problem for relativistic particles is roughly similar. Dynamics is now described by the Bethe-Salpeter equation and its *kernel* corresponds to the potential. In the case of scattering of two generic particles X and Y, this kernel amounts to the sum of all *proper* intermediate diagrams, that is, those which cannot be split into two pieces by cutting X and Y propagators only. Similarly to what happens with the potential, real kernels give rise to elastic interactions, whereas inelasticities require complex kernels.

In quantum mechanics, the so called inverse problem, in which one attempts to derive potentials from scattering amplitudes, has been widely studied and one knows that it does not have unique solutions. The same holds for the relationship between scattering amplitudes and kernels, in the framework of relativity. This problem has been discussed long ago by Lang[3], who has shown that constraints imposed by unitarity on scattering amplitudes cannot fix kernels completely. However, in the case of low and medium energy meson-meson scattering, the Bethe-Salpeter equation can be simplified and there is a window in which an approximate solution to the inverse problem does exist, which we discuss in the sequence. In the last two decades, this simplification of the Bethe-Salpeter has been extensively used in the dynamical unitarization of amplitudes and successfully applied to a wide number of problems[4, 5].

Quite generally, the reaction $X(p_x)\,Y(p_y) \to X(p'_x)\,Y(p'_y)$ is described in terms of Mandelstam variables s, t, u and, in the center of mass system (CM), results can be expressed in terms of the three-momentum $\boldsymbol{q}$, with $\boldsymbol{q}^2 = s\,\rho^2/4$,

$$\rho = \sqrt{1 - 2\,(m_x^2+m_y^2)/s + (m_x^2-m_y^2)^2/s^2}\,. \tag{1}$$

The corresponding amplitude T_{xy} can be formally represented in terms of the Bethe-Salpeter equation as

$$T_{xy}(s) \;=\; \mathcal{K}_{xy}(s) - i\int \frac{d^4\ell}{(2\pi)^4}\;\frac{\mathcal{K}_{xy}(P,\ell)\;\;T_{xy}(P,\ell)}{[(\ell+P/2)^2-m_x^2+i\,\epsilon\,]\;[(\ell-P/2)^2-m_y^2+i\,\epsilon\,]}\;, \tag{2}$$

where K_{xy} is the kernel and $P = p_x + p_y$. This equation can be simplified if one assumes that, at low energies, the dependences of both $\mathcal{K}_{xy}(P,\ell)$ and $T_{xy}(P,\ell)$ on the loop variable ℓ can be neglected. This assumption has been used in Ref.[3], tested in many instances[4, 6], and allows the amplitude to be written as

$$T_{xy}(s) = \mathcal{K}_{xy}(s)\;\;[1 - T_{xy}(s)\;\Omega_{xy}(s)]\;\;, \tag{3}$$

where the function

$$\Omega_{xy}(s) = i\int \frac{d^4\ell}{(2\pi)^4}\;\frac{1}{[(\ell+P/2)^2 - m_x^2\,]\;[(\ell-P/2)^2 - m_y^2\,]} \tag{4}$$

represents the elastic two-particle XY propagator, shown in fig.1.

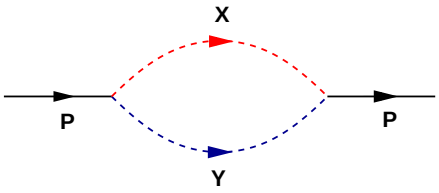

FIG. 1: Light two-particle propagator.

The integral (4) is ultraviolet divergent and a subtraction is needed. Following ref.[7], we write the regular part of Ω_{xy} as

$$\bar{\Omega}_{xy}(s) = \Omega_{xy}(s) - \Omega_{xy}(0)\;, \tag{5}$$

where the divergent part is contained in $\Omega_{xy}(0)$. Regularization amounts to replacing this term by an unknown finite constant C, which has to be fixed later. The function $\bar{\Omega}$ can be

evaluated analytically and, above threshold, one has

$$\bar{\Omega}_{xy}(s) = (\bar{\Omega}_{xy})_R + i\,(\bar{\Omega}_{xy})_I = -\bar{L}_{xy}(s)/(S_{xy}\,16\pi^2)\;, \tag{6}$$

$$\begin{aligned}\bar{L}_{xy} &= 1 + \frac{m_x^2+m_y^2}{m_x^2-m_y^2}\;\ln\left[\frac{m_x}{m_y}\right] - \frac{m_x^2-m_y^2}{s}\;\ln\left[\frac{m_x}{m_y}\right] \\ &- \frac{\sqrt{\lambda}}{s}\;\ln\left[\frac{s-m_x^2-m_y^2+\sqrt{\lambda}}{2\,m_x\,m_y}\right] + i\,\pi\,\frac{\sqrt{\lambda}}{s}\;,\end{aligned} \tag{7}$$

with $\sqrt{\lambda} = s\,\rho$ and S_{xy}, the symmetry factor, is 1 for $X \neq Y$ and 2 for $X = Y$. After regularization, eq.(3) may be solved for T_{xy} and one finds[3]

$$T_{xy}(s) = \frac{\mathcal{K}_{xy}(s)}{1 + [\bar{\Omega}_{xy}(s)+C]\;\mathcal{K}_{xy}(s)}\;. \tag{8}$$

In the elastic regime, the kernel $\mathcal{K}_{xy}$ is real and the complex structure of eq.(7) makes T_{xy} automatically unitary. On the other hand, when inelasticities are present, the kernel $\mathcal{K}_{xy}$ acquires imaginary components. The conceptual relationship between the amplitude and the kernel can be better understood by rewriting eq.(8) as the geometric series

$$\begin{aligned}T_{xy}(s) &= \mathcal{K}_{xy}(s) - \mathcal{K}_{xy}(s)\,[\bar{\Omega}_{xy}(s)+C]\,\mathcal{K}_{xy}(s) \\ &+ \mathcal{K}_{xy}(s)\,[\bar{\Omega}_{xy}(s)+C]\,\mathcal{K}_{xy}(s)\,[\bar{\Omega}_{xy}(s)+C]\,\mathcal{K}_{xy}(s) + \cdots\;.\end{aligned} \tag{9}$$

This shows that the amplitude is just a monotonous iteration of the kernel, as shown in fig.2. It is therefore desirable to know the kernel, since it encompasses all relevant dynamical effects.

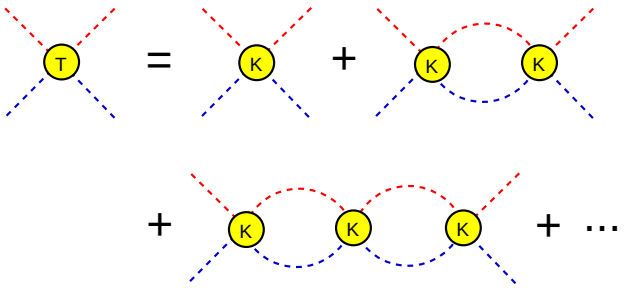

FIG. 2: Amplitude for the process $XY \to XY$ represented as a geometric series involving the kernel $\mathcal{K}$ and light-meson propagators.

Data are usually presented by means of a non-relativistic amplitude f, which can be parametrized in terms of either phase and modulus or phase and elasticity, and related with

the relativistic amplitude T by

$$\frac{\rho\, T_{xy}}{16\pi} = f_{xy} = |\, f_{xy}\,|\, e^{i\,\delta_{xy}} = \frac{1}{2i}\left[\eta_{xy} e^{2i\bar{\delta}_{xy}} - 1\right] \ . \tag{10}$$

Feeding the experimental amplitude T^{exp}_{xy}, extracted from eq.(10), into eq.(8), and inverting it, one finds a solution to the inverse problem, given by

$$\mathcal{K}^{exp}_{xy}(s) = \frac{T^{exp}_{xy}(s)}{1 - [\bar{\Omega}_{xy}(s) + C]\; T^{exp}_{xy}(s)} \ . \tag{11}$$

As we discuss in the sequence, this function $\mathcal{K}^{exp}_{xy}$ conveys dynamical information in a very transparent way, since it is free from XY intermediate states. It rests at the basis of the procedure proposed here.

In order to evaluate eq.(11), one needs to fix the constant C. Since it cannot be fixed directly from data, it must be taken as a free parameter and the function $\mathcal{K}^{exp}_{xy}$ is contaminated by this freedom. However, once a choice is made, the kernel is uniquely determined and its use in eq.(8) yields results which do not depend on conventions. The choice made in Ref.[3] corresponds to $C = 0$. Here, we fix C by noting that, at the the point $s = s_{\pi/2}$, for which $\delta_{xy}(s_{\pi/2}) = \pi/2$, one has $T_{xy}(s_{\pi/2}) = i\, 16\pi/\rho(s_{\pi/2})$. Using this, together with the result $(\bar{\Omega}_{xy})_I = -\rho/16\pi$, one finds

$$\mathcal{K}^{exp}_{xy}(s_{\pi/2}) = -\,\frac{1}{[\bar{\Omega}_{xy}(s_{\pi/2})]_R + C} \ . \tag{12}$$

One then chooses $C = -[\bar{\Omega}_{xy}(s_{\pi/2})]_R$, because this gives rise to a pole in $\mathcal{K}^{exp}_{xy}(s_{\pi/2})$, correlated with the phase $\delta_{xy}(s_{\pi/2}) = \pi/2$ and associated with a light resonance R_L in the XY channel, of mass $m_{R_L} = \sqrt{s_{\pi/2}}$.

As far as theory is concerned, it is useful to decompose the kernel $\mathcal{K}$ into light and heavy pieces, denoted by $\mathcal{K}_L$ and $\mathcal{K}_H$, as in Fig.3. The latter includes interactions of heavy systems and is discussed in App.B. The light component $\mathcal{K}_L$ is real and involves only light-particles. In the framework of chiral models[10], this light kernel is given by the sum of a leading contact term, a light bare s-channel resonance R_L, and corrections associated with exchanges of resonances in t- and u-channels. We stress, however, that the use of a chiral model is not compulsory. The only essential ingredient in K_L is the light resonance, whereas the other terms could well be replaced by a polynomial in s, with free coefficients. In order to stress this feature it is convenient to express the light kernel as

$$\mathcal{K}_L = \mathcal{K}_{R_L} + \mathcal{K}_{BG_L} \ . \tag{13}$$

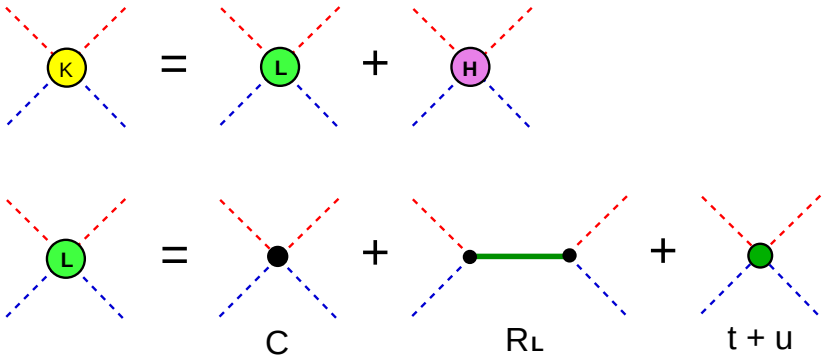

FIG. 3: Top: decomposition of the kernel $\mathcal{K}$ into light and heavy components $\mathcal{K}_L$ and $\mathcal{K}_H$. Bottom: chiral model for $\mathcal{K}_L$, based on a leading contact interaction (C), a bare s-channel light resonance (R_L) and correction terms ($t+u$).

Hence the theoretical kernel reads

$$\mathcal{K}^{th}_{xy} \equiv \mathcal{K}_{R_L} + \mathcal{K}_{BG_L} + \mathcal{K}_H \ , \tag{14}$$

The form of the bare resonance term $\mathcal{K}_{R_L}$ is given in App.A and a chiral model for $\mathcal{K}_{BG_L}$, suited to the $K\pi$ system, is presented in App.C.

II. $K\pi$ AMPLITUDE

The preceding discussion, which is somewhat abstract, can be made more concrete with the help of a guiding instance. With this purpose in mind, we present the case of $K\pi$ scattering, for which data is available[8] in the range $0.825 < E < 1.960$ GeV, and concentrate on the P-wave channel with isospin 1/2. Data for this channel indicate that $\sqrt{s_{\pi/2}} = 0.894\,\text{GeV}$, which corresponds to the mass of the $K^*(892)$.

In fig.4 we show the central values for real and imaginary components of the amplitude $T^{exp}_{K\pi}$ and, in fig.5, the counterparts for $\mathcal{K}^{exp}_{K\pi}$, obtained by using these values into eq.(11). Comparing both figures in the region around m_{K^*}, one notes a behaviour similar to a Breit-Wigner function (BWF) for the amplitude and a bare pole for the kernel. This is to be expected, since eq.(8) does indeed transform bare poles into Breit-Wigner functions and, in this process, a resonance in the elastic regime acquires its width, through coupling to K and π states. The kernel associated with m_{K^*} and the corresponding BWF are shown in fig.6. In the case of P-waves, the kernel describing the propagation of a single vector resonance is

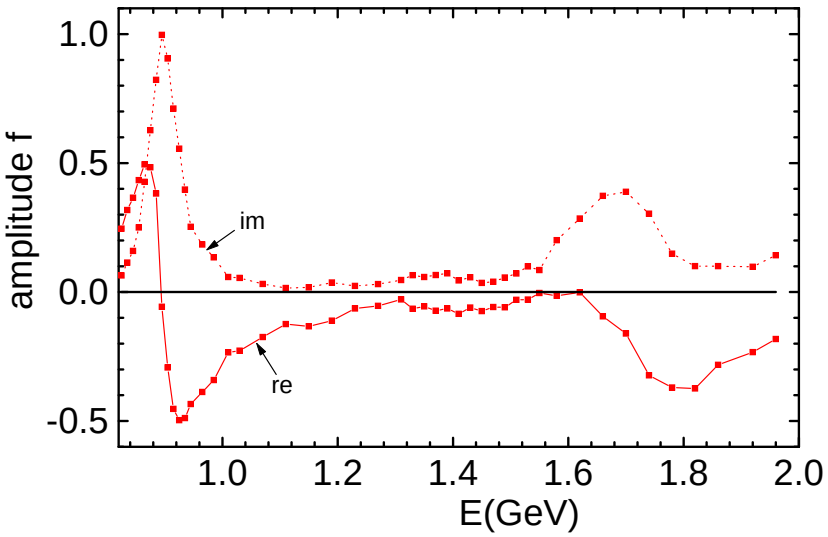

FIG. 4: Real and imaginary components of experimental function $f_{K\pi}$, eq.(10); lines were added to guide the eye.

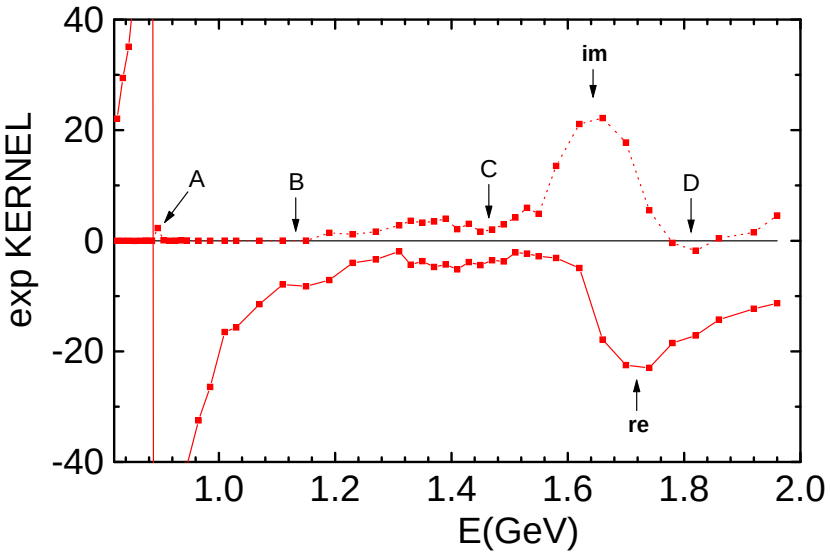

FIG. 5: Real and imaginary components of the function $\mathcal{K}^{exp}_{K\pi}$, eq.(11); lines were added to guide the eye.

presented in appendix A. In the framework of the $K\pi$ system, eq.(A5) reads

$$\mathcal{K}_{R_L} = \mathcal{K}_{K^*} = -\left\{g_{K^*}\left|\boldsymbol{q}\right|\right\}^2 \frac{s}{s-m^2_{K^*}}\,, \tag{15}$$

where $g_{K^*} = G_V/F^2$ is the $K^*K\pi$ coupling constant[10]. When a structure of this kind is used into eq.(8), one gets a typical Breit-Wigner amplitude. The width of this resonance is directly proportional to $g^2_{K^*}$, stressing its dynamic origin.

This pattern is fully backed by field theory. Effective lagrangians, suited to describing low energy mesonic interactions, have been intensively studied in the last three decades[7, 9] and the treatment of resonances has been thoroughly discussed in ref.[10]. Within the lagrangian formalism, the only intrinsic property of a resonance is its mass, which is a real parameter. The width is not intrinsic and has to be generated dynamically, by means of couplings to possible decay products.

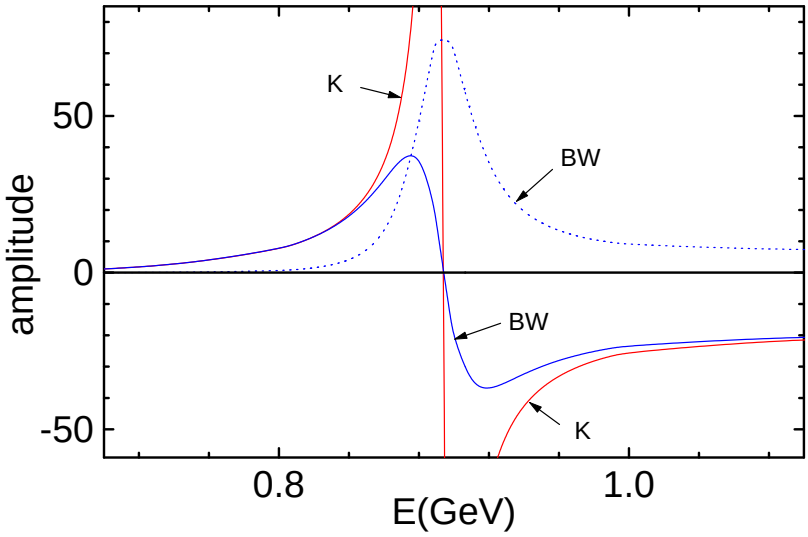

FIG. 6: Kernel (K, red curve) and real (BW, blue continuous curve) and imaginary (BW, blue dotted curve) components of the Breit-Wigner amplitude associated with the $K^*(892)$.

The elimination of $K\pi$ intermediate states from data yields the kernel $\mathcal{K}^{exp}_{K\pi}$, shown in fig.5, where the $K^*(892)$ pole in the real component is clearly visible, at point A. Inspecting the imaginary component, one learns that it vanishes up to point B, indicating the higher end of the elastic regime. From that region onwards, reactions such as $K\,\pi \to K^*\,\pi$ or $K\,\pi \to K\,\rho$ become possible[11]. At higher energies, one finds at least two bumps, associated with resonances. One might also be tempted to interpret data beyond point D as the tail of a third bump. As loops are the only source of imaginary components in hadronic field theory, an imaginary part in $\mathcal{K}^{exp}_{K\pi}$ is a clear indication of the presence of loops involving heavy intermediate states.

The extraction of information from bumps in the imaginary component requires some theory, since one has to understand how basic dynamics allows several resonances to get dressed. A somewhat detailed discussion of this subject can be found in appendix B. Results

given there are consistent with unitarity indicating that, as expected, the imaginary part of $\mathcal{K}^{exp}_{K\pi}$ cannot be negative. Inspecting the region close to point D in fig.5, one learns that a problem with data may be present there. A comprehensive fit function for $\mathcal{K}_H$, the heavy component of the kernel, is given in eq.(B8). However, this function is complicate and we consider two simpler limits, whereby either each resonance develops its own imaginary part independently or this is a fully collective process. The former case corresponds to the direct sum of two Breit-Wigner functions, given by eq.(B9), and the latter, to eq.(B10), in which bare propagators are added before the unitarization procedure. The distinctive feature of the kernel given by eq.(B10) is that it has to vanish at a point at the right of the first peak, as shown in fig.14. This could, in principle, be useful for describing the region around point D in fig.5.

In our $K\pi$ instance, the structure of the function $\mathcal{K}_H$ has been chosen as a combination of eqs.(B9) and (B10), which reads

$$\mathcal{K}_H = |\boldsymbol{q}|^2 \left\{ \lambda_a^2 \, \frac{\Delta_a}{1 - i\, g_a^2\, \Delta_a\, |\boldsymbol{Q}_1|^3/8\pi\sqrt{s}} + \xi^2 \, \frac{g_b^2\, \Delta_b + g_c^2\, \Delta_c}{1 - i\, [g_b^2\, \Delta_b + g_c^2\, \Delta_c]\, |\boldsymbol{Q}_2|^3/8\pi\sqrt{s}} \right\} \, , \qquad (16)$$

where λ_a , ξ , and the g_i are free parameters and

$$\Delta_i = - \, \frac{s}{s - m_i^2} \, . \qquad (17)$$

The denominators in eq.(16) are complex and the same happens with the entire function $\mathcal{K}_H$. This choice was motivated by fig.5, since it seems to describe a broad resonance at energies around 1.4 GeV, associated with Δ_a, and a dip around 1.8 GeV, associated with the weighted sum of Δ_b and Δ_c.

A possible model for the real background function $\mathcal{K}_{BG_L}$ is given in appendix C. It receives contributions from a contact interaction $\mathcal{K}^C_L$, associated with chiral symmetry[7], and exchanges of scalar and vector resonances in t and u channels, denoted by $\mathcal{K}^S_L$ and $\mathcal{K}^V_L$. Our trial function for the light part of the kernel is written as

$$\mathcal{K}_L = \mathcal{K}_{K^*} + \mathcal{K}_{BG_L} = \mathcal{K}^C_L + \alpha \, \left[- \frac{G_V^2}{F^4} \, \frac{s\, |\boldsymbol{q}|^2}{s - m^2_{K^*}} + \mathcal{K}^V_{K^*} \right] + \beta \, \mathcal{K}^V_{L\rho} + \gamma \, \mathcal{K}^S_L \, , \qquad (18)$$

where α, β and γ are free parameters.

Using the structures given by eqs.(16) and (18), we fitted the phase and modulus for the P-wave $K\pi$ amplitude with isospin 1/2 and the results are given in fig.7. We also obtained the couple of functions phase-inelasticity as given in fig.8. The fit information and the values

for free parameters can be found in appendix D. In spite of the fact that data may have problems around point D of fig.(5), these results can be considered as being satisfactory.

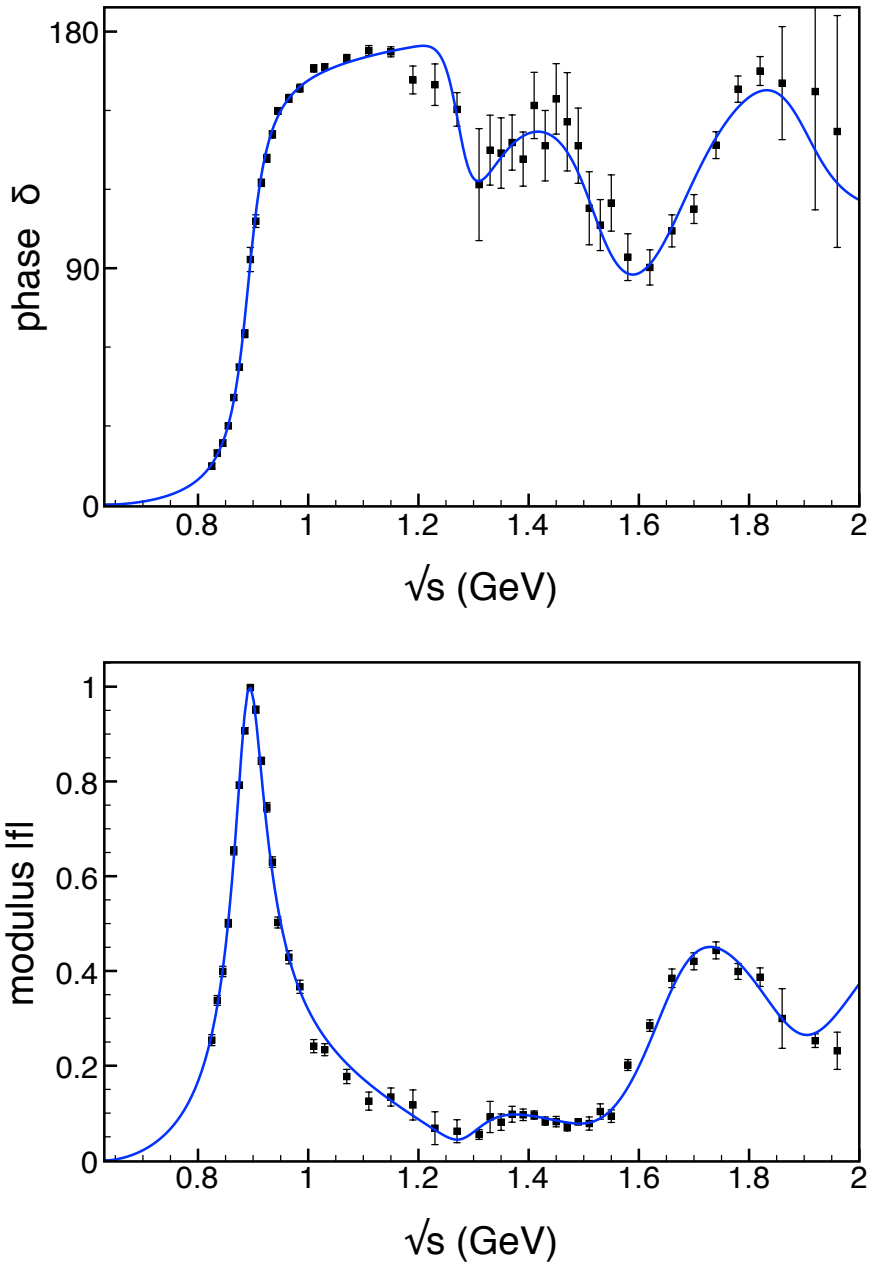

FIG. 7: Results for the phase δ (top) and modulus $|f|$(bottom) of the fitted $K\pi$ amplitude, using eqs (16) and (18), compared with data[8]. The $\chi^2/n.d.f.$ of the fit is 2.13 for the phase and 5.16 for the modulus.

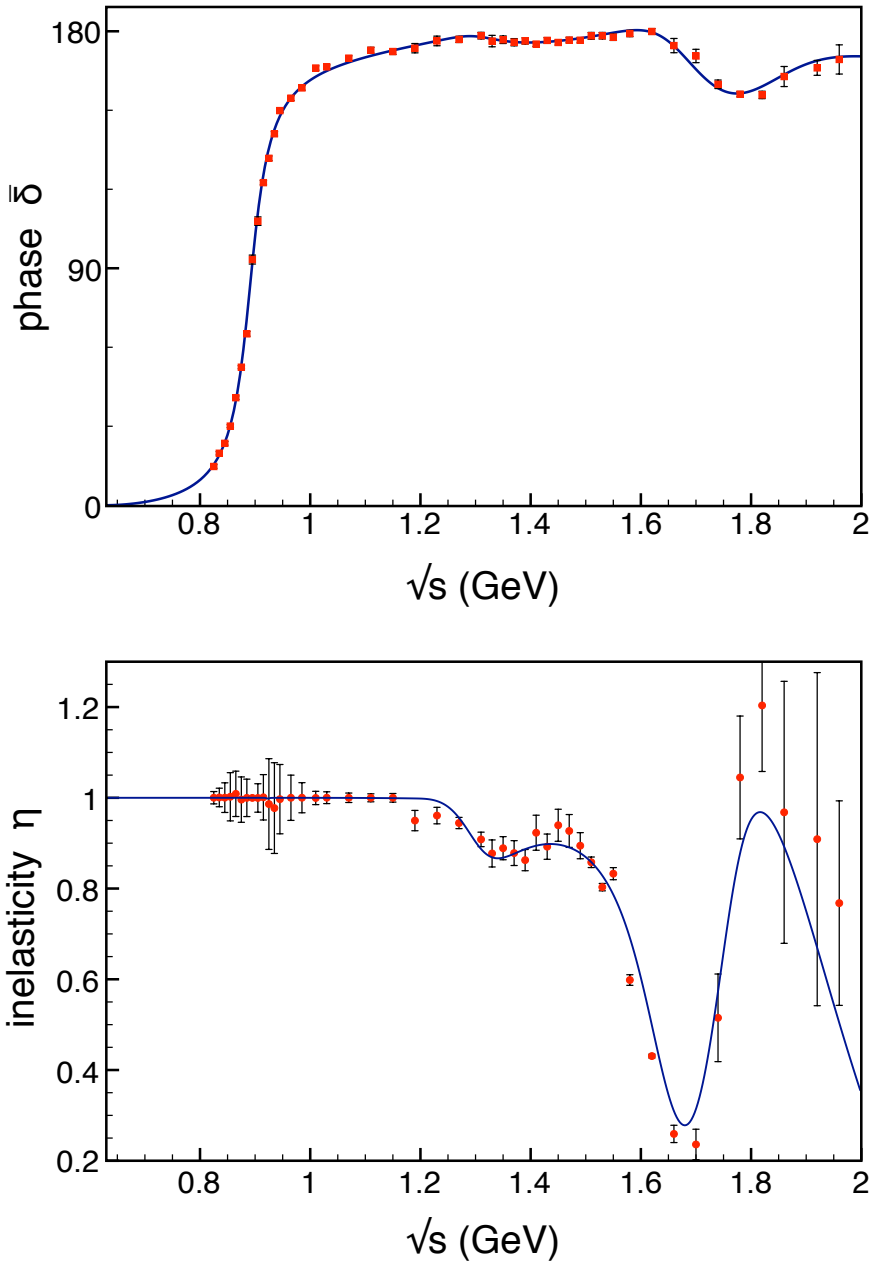

FIG. 8: Results for the phase $\bar{\delta}$ and inelasticity η of the fitted $K\pi$ amplitude, using eqs (16) and (18).

III. SUMMARY

We described a procedure which may be instrumental in analyses of low and medium energy hadronic scattering data. The basic idea is that $\mathcal{K}$, the kernel of the system, which conveys dynamical information, has a much simpler and transparent structure than the amplitude T. In particular, Breit-Wigner trial functions are much more suited to describing

the relatively small complex structures associated with possible inelasticities rather than the full interplay between real and imaginary components of the amplitude.

The basic steps of this procedure are summarized below. In the generic process $XY \to XY$, one departs from the scattering amplitude T_{xy}^{exp} taken from data and, using the XY propagator $\bar{\Omega}_{xy}$, given by eqs.(6) and (7), into eq.(11), derives a representation for the experimental kernel $\mathcal{K}_{xy}^{exp}$. This function, in turn, can be decomposed as in eq.(14), which reads

$$\mathcal{K}_{xy}^{th} \equiv \mathcal{K}_{R_L} + \mathcal{K}_{BG_L} + \mathcal{K}_H \ ,$$

where $\mathcal{K}_{R_L}$ is real, contains the pole of the lowest resonance, and can be fixed by the neighbourhood of the point at which the phase reaches 90^0. The term $\mathcal{K}_H$ is complex, conveys information about heavier resonances, and can be represented as a combination of Breit-Wigner functions suited to the case. Finally, $\mathcal{K}_{BG_L}$ is a real contribution which may be either fitted by a polynomial or associated with a model. Once the kernel $\mathcal{K}_{xy}^{th}$ is known, the full complex structure of the amplitude is recovered by using eq.(8).

ACKNOWLEDGMENTS

The work of P.C.M. was supported by Fundação de Amparo à Pesquisa do Estado de São Paulo (FAPESP).

Appendix A: vector amplitude

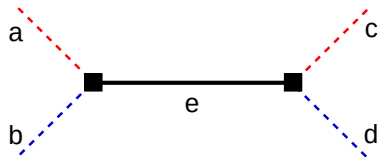

FIG. 9: Kernel involving an intermediate vector resonance.

In the framework of $SU(3)$, the s-channel tree amplitude $T_{ab\to cd}$, describing the reaction among pseudoscalars $P_a(p_a)\,P_b(p_b) \to P_c(p_c)\,P_d(p_d)$, mediated by a vector resonance V_e of mass m_e is given by[10]

$$T_{ab\to cd} = -f_{abe}\,f_{cde}\,G_{abe}\,G_{cde}\,\frac{1}{s-m_e^2} \times \left[2\,s\,t + s^2 - s\,(M_a^2+M_b^2+M_c^2+M_d^2) + (M_a^2-M_b^2)\,(M_c^2-M_d^2)\right]\,, \tag{A1}$$

where the f_{ijk} are $SU(3)$ structure constants and the G_{ijk} are coupling constants. In the center of mass frame, this result can be rewritten in terms of initial and final tree-momenta $\boldsymbol{q}$ and $\boldsymbol{Q}$ as

$$T_{ab\to cd} = -f_{abe}\,f_{cde}\,G_{abe}\,G_{cde}\,\frac{4\,s}{s-m_e^2}\,\boldsymbol{q}\cdot\boldsymbol{Q}\,, \tag{A2}$$

$$\boldsymbol{q} = \frac{1}{2\sqrt{s}}\sqrt{s^2 - 2s\,(M_a^2+M_b^2) + (M_a^2-M_b^2)^2}\,, \tag{A3}$$

$$\boldsymbol{Q} = \frac{1}{2\sqrt{s}}\sqrt{s^2 - 2s\,(M_c^2+M_d^2) + (M_c^2-M_d^2)^2}\,. \tag{A4}$$

Projecting out the P-wave, one finds the typical structure for the kernel, which is given by

$$\mathcal{K}_{ab\to cd} = -\,\{g_{abe}\,|\boldsymbol{q}|\,\}\;\{g_{cde}\,|\boldsymbol{Q}|\,\}\;\frac{s}{s-m_e^2}\,, \tag{A5}$$

where a factor 4/3 and the structure constants f_{ijk} have been absorbed into the new coupling constants g_{ijk}.

In the case $X=a=c$, $Y=b=d$, this result represents the s-channel pole of the bare light resonance R_L, shown in Fig.3. Its contribution to the light kernel $\mathcal{K}_L$ is

$$\mathcal{K}_{R_L} = \{g_{R_L}\,|\boldsymbol{q}|\,\}^2\;\Delta_{R_L}\,, \tag{A6}$$

$$\Delta_{R_L} = -\,\frac{s}{s-m_{R_L}^2}\,, \tag{A7}$$

where g_{R_L} is the XYR_L coupling constant and $\boldsymbol{q}$ is given by eq.(A3). The iteration of this kernel, as in Fig.2, gives rise to a geometric series, whose sum is indicated by $\bar{\mathcal{K}}_{R_L}$ and reads

$$\bar{\mathcal{K}}_{R_L} = \{g_{R_L}\,|\boldsymbol{q}|\,\}\,\{\bar{\Delta}_{R_L}\}\,\{g_{R_L}\,|\boldsymbol{q}|\,\}\ , \tag{A8}$$

$$\bar{\Delta}_{R_L} = \{\Delta_{R_L} - \Delta_{R_L}[U_{xy}]\Delta_{R_L} + \Delta_{R_L}[U_{xy}]\Delta_{R_L}[U_{xy}]\Delta_{R_L} + \cdots\}\ , \tag{A9}$$

$$U_{R_L} = \{g_{R_L}\,|\boldsymbol{q}|\,\}\,(\bar{\Omega}_{xy}+C)\,\{g_{R_L}\,|\boldsymbol{q}|\,\}\ , \tag{A10}$$

where $\bar{\Delta}_{R_L}$ is the dressed resonance propagator. Summing the series (A9) and using eq.(A7), one may express it as

$$\bar{\Delta}_{R_L} = \frac{\Delta_{R_L}}{1 + U_{R_L}\,\Delta_{R_L}} = -\,\frac{s}{s - m^2_{R_L} - U_{R_L}\,s}\ , \tag{A11}$$

indicating that the resonance has been dressed. The real part of U_{R_L} influences its mass and the imaginary part gives rise to its width.

Appendix B: heavy resonances

The amplitude describing the generic elastic reaction $XY \to XY$ is given by the geometric series displayed in Fig.2 and involves both light and heavy kernels, as indicated in Fig.3. The light loop, shown in fig.1, involves just particles X and Y themselves and is described by the function $\bar{\Omega}_{xy}$ given in eq.(6).

In this Appendix we describe the structure of the heavy kernel $\mathcal{K}_H$, which encompasses all heavy loops, that is, those different from the light one. In order to make our discussion more concrete, we assume that heavy loops represent the propagation of excited states, such as XY^* and X^*Y. This assumption simplifies the presentation, but results do not depend on it and remain valid if other intermediate states are included.

In $\mathcal{K}_H$, the incoming and outgoing light particles X and Y couple to heavy systems, which are assumed to be *proper*, in the sense that they cannot be split into two parts by cutting intermediate X and Y lines only. These heavy systems contain heavy loops, that give rise to complex components into $\mathcal{K}_H$.

The expression for $\mathcal{K}_H$, in the case of a single heavy resonance R_a, coupled to a single intermediate heavy loop propagator ω_1, is a direct generalization of eqs.(A8-A10) and given by

$$\mathcal{K}_H = \mathcal{K}_a = \{\lambda_a\,|\boldsymbol{q}|\,\}\,\{\bar{\Delta}_a\}\,\{\lambda_a\,|\boldsymbol{q}|\,\}\ , \tag{B1}$$

$$\bar{\Delta}_a = \{\Delta_a - \Delta_a\, U_{aa}\, \Delta_a + \Delta_a\, U_{aa}\, \Delta_a\, U_{aa}\, \Delta_a + \cdots\} = \frac{\Delta_a}{1 + U_{aa}\, \Delta_a}\ , \tag{B2}$$

$$U_{aa} = \{g_{a1}\, |\boldsymbol{Q}_1|\}\, \{\omega_1\}\, \{g_{a1}\, |\boldsymbol{Q}_1|\}\ , \tag{B3}$$

where λ_a is the $R_a XY$ coupling constant, g_{a1} is the coupling constant of R_a to the heavy loop and the variable $\boldsymbol{Q}_1$ is three-momentum inside the heavy loop. In case the resonance can couple to two different intermediate states, labelled by 1 and 2, eq.(B3) becomes

$$U_{aa} = \{g_{a1}\, |\boldsymbol{Q}_1|\}\ \{\omega_1\}\, \{g_{a1}\, |\boldsymbol{Q}_1|\} + \{g_{a2}\, |\boldsymbol{Q}_2|\}\, \{\omega_2\}\, \{g_{a2}\, |\boldsymbol{Q}_2|\} \tag{B4}$$

and is illustrated in Fig.10, for XY^* and X^*Y intermediate states.

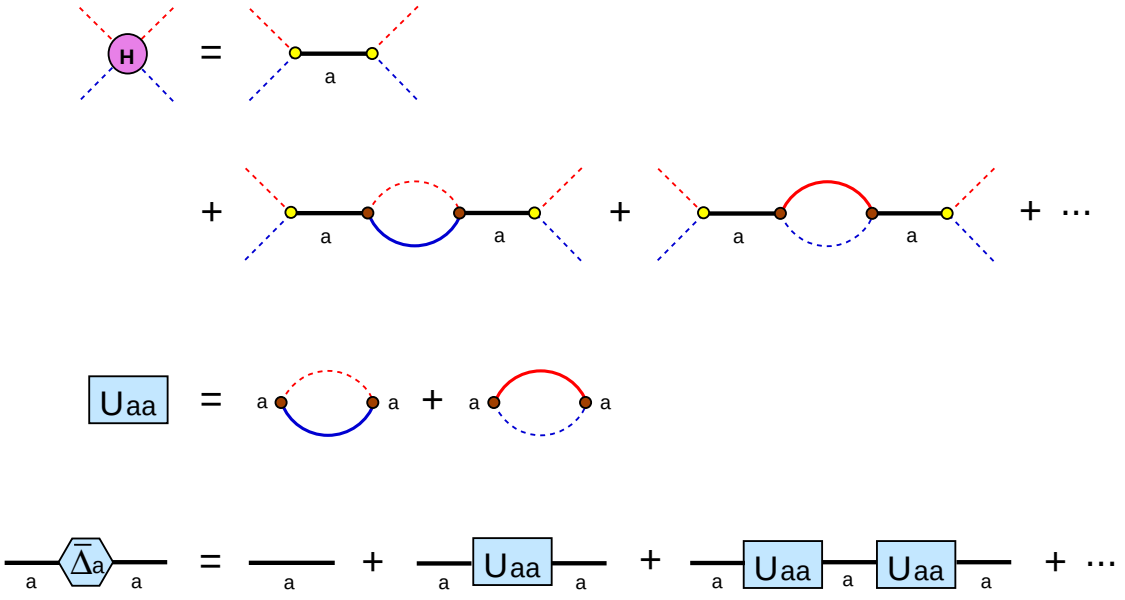

FIG. 10: Top: heavy kernel for a single resonance R_a; continuous lines in the loops represent excited states X^* or Y^*, whereas the couplings λ_a and g_{a1} are indicated respectively by open yellow and black circles. Center: heavy loop function U_{aa}. Bottom: R_a propagator dressed by heavy loops.

The inclusion of a second resonance R_b into the problem gives rise to oscillations, due to mixed couplings of the form

$$U_{ab} = \{g_{a1}\, |\boldsymbol{Q}_1|\}\ \{\omega_1\}\, \{g_{b1}\, |\boldsymbol{Q}_1|\} + \{g_{a2}\, |\boldsymbol{Q}_2|\}\, \{\omega_2\}\, \{g_{b2}\, |\boldsymbol{Q}_2|\}\ . \tag{B5}$$

The full propagator describing a resonance R_a, which oscillates and still ends up as a resonance R_a, is represented in Fig.11 and corresponds to the series

$$\begin{aligned} \boldsymbol{\Delta}_{aa} &= \bar{\Delta}_a + \bar{\Delta}_a\, U_{ab}\, \bar{\Delta}_b\, U_{ba}\, \bar{\Delta}_a + \bar{\Delta}_a\, U_{ab}\, \bar{\Delta}_b\, U_{ba}\, \bar{\Delta}_a\, U_{ab}\, \bar{\Delta}_b\, U_{ba}\, \bar{\Delta}_a + \cdots \\ &= \frac{\bar{\Delta}_a}{1 - U_{ab}^2\, \bar{\Delta}_a\, \bar{\Delta}_b}\ . \end{aligned} \tag{B6}$$

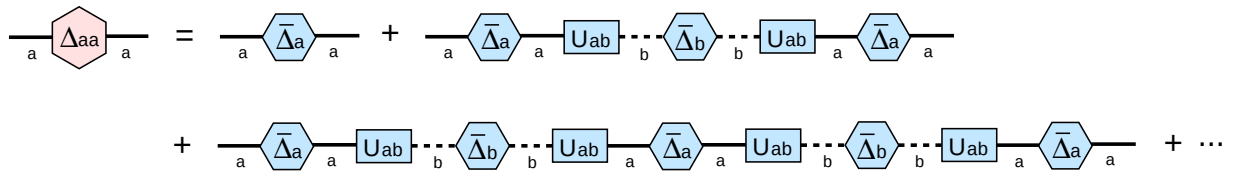

FIG. 11: R_a propagator dressed by heavy loops and including forth and back oscillations into R_b.

The propagator for a state R_a, which oscillates and becomes a state R_b, is obtained by multiplying eq.(B6) by $-U_{ab}\,\bar{\Delta}_b$ and reads

$$\begin{aligned}\mathbf{\Delta}_{ab} &= -\bar{\Delta}_a U_{ab}\,\bar{\Delta}_b - \bar{\Delta}_a\,U_{ab}\,\bar{\Delta}_b\,U_{ba}\,\bar{\Delta}_a\,U_{ab}\,\bar{\Delta}_b - \bar{\Delta}_a\,U_{ab}\,\bar{\Delta}_b\,U_{ba}\,\bar{\Delta}_a\,U_{ab}\,\bar{\Delta}_b\,U_{ba}\,\bar{\Delta}_a\,U_{ab}\,\bar{\Delta}_b + \cdots \\ &= -\mathbf{\Delta}_{aa}\,U_{ab}\,\bar{\Delta}_b = -\,\frac{\bar{\Delta}_a\,U_{ab}\,\bar{\Delta}_b}{1-U_{ba}^2\,\bar{\Delta}_a\,\bar{\Delta}_b}\,. \end{aligned} \tag{B7}$$

The heavy component of the kernel is then given by the diagrams of Fig.12, which correspond to

$$\mathcal{K}_H = |\boldsymbol{q}|^2\,\frac{\lambda_a^2\,\bar{\Delta}_a + \lambda_b^2\,\bar{\Delta}_b - 2\,\lambda_a\,\lambda_b\,\bar{\Delta}_a\,U_{ab}\,\bar{\Delta}_b}{1-U_{ba}^2\,\bar{\Delta}_a\,\bar{\Delta}_b}\,. \tag{B8}$$

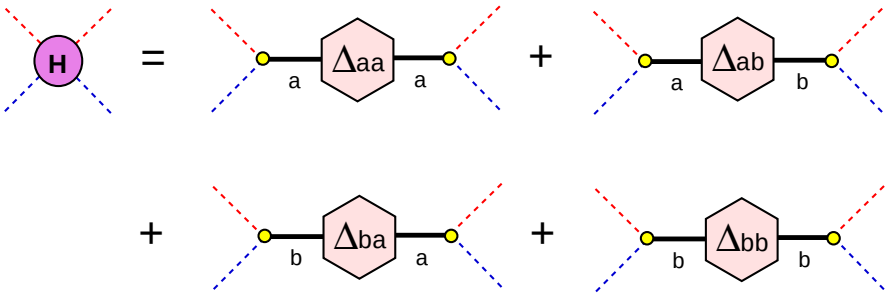

FIG. 12: Full heavy kernel $\mathcal{K}_H$.

This result is comprehensive but may be too involved to be used as a practical fit function. We therefore consider two kinds of simplifications, among many other possible. The first one consists in neglecting oscillations between R_a and R_b, by making $g_{a2} = g_{b1} = 0$. This yields $U_{ab} \to 0$ and

$$\mathcal{K}_H \simeq |\boldsymbol{q}|^2\,\left[\lambda_a^2\,\bar{\Delta}_a + \lambda_b^2\,\bar{\Delta}_b\right]\,, \tag{B9}$$

which represents a simple sum of independent Breit-Wigner functions. Owing to its simplicity, this choice is often made in data analyses and sometimes refered to as *isobaric model*.

In the second approximation, the coupling between R_a and R_b is kept, but one assumes $g_{a2} = g_{b2} = 0$, $\lambda_a = \xi\, g_{a1}$ and $\lambda_b = \xi\, g_{b1}$. This gives rise to

$$\mathcal{K}_H \simeq \xi^2\, |\boldsymbol{q}|^2\, \frac{g_{a1}^2\, \Delta_a + g_{b1}^2\, \Delta_b}{1 + \omega_1\, \boldsymbol{Q}_1^2\, [g_{a1}^2\, \Delta_a + g_{b1}^2\, \Delta_b]}\ . \tag{B10}$$

The signature of this pattern of composition is that the complex function $\mathcal{K}_H$ has to vanish at $s = (g_{a1}^2 m_b^2 + g_{b1}^2 m_a^2)/(g_{a1}^2 + g_{b1}^2)$.

The use of the so called K-matrix approximation yields a complementary useful simplification for $\mathcal{K}_H$. It amounts to assuming that intermediate particles are on-shell and neglecting real parts of heavy propagators. This corresponds to employing

$$\omega_i \simeq i\, [\omega_1]_I = -i\, \frac{\boldsymbol{Q}_i}{8\pi\sqrt{s}}\ . \tag{B11}$$

We conclude by discussing the main qualitative features of results presented. In fig.13 we show the behaviour of the single resonance propagator, given by eq.(B2), for two different values of the coupling constant g_{a1}. The zero of the real parts occur at $s = m_a^2$, where the imaginary parts reach their maxima. It is worth noting that the imaginary components are not symmetric around this point.

Consequences from the approximation associated with eq.(B10) can be seen in the curves of fig.14 where, for the sake of comparison, the case of a single resonance is also shown in curves b. The whole two-resonance propagator vanishes at point P, where the real component crosses the axis and the imaginary component just touches it, since it cannot be negative. This kind of pattern for the imaginary part might, in principle, be related with the behaviour of $\mathcal{K}_{K\pi}^{exp}$, at point D of fig.5. It is interesting to compare the imaginary parts of curves a and b around the first peak for, even there, the influence of the second resonance can be seen.

Appendix C: background $K\pi$ amplitude

We describe below a possible model suited to the case of elastic $K\pi$ scattering, inspired in chiral perturbation theory[7, 10]. The regular part of the background kernel, which is real, is assumed to be given by

$$\mathcal{K}_{BG_L} = \mathcal{K}_L^C + \mathcal{K}_L^S + \mathcal{K}_L^V\ , \tag{C1}$$

where $\mathcal{K}_L^C$ is a leading order contact interaction, whereas $\mathcal{K}_L^S$ and $\mathcal{K}_L^V$ are corrections due to t- and u-channel exchanges of scalar and vector resonances. Using the notation of ref.[10],

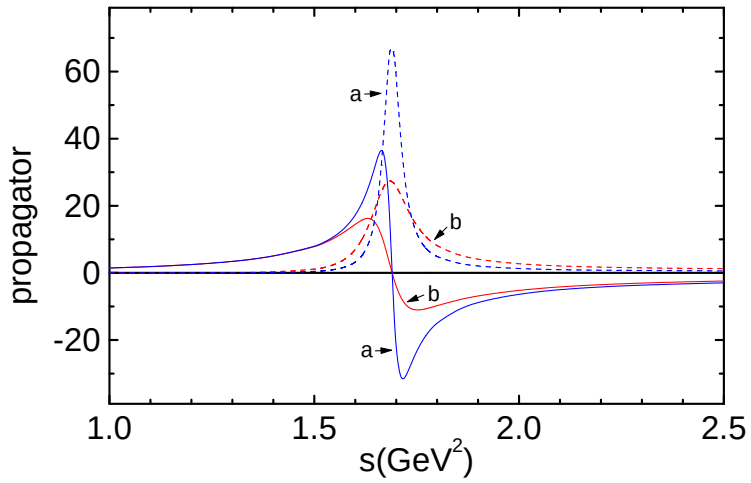

FIG. 13: Real (continuous line) and imaginary (dashed line) components of the single resonance propagator given by eq.(B2) for two different values (a,b) of the coupling constant g_{a1}; scales are arbitrary.

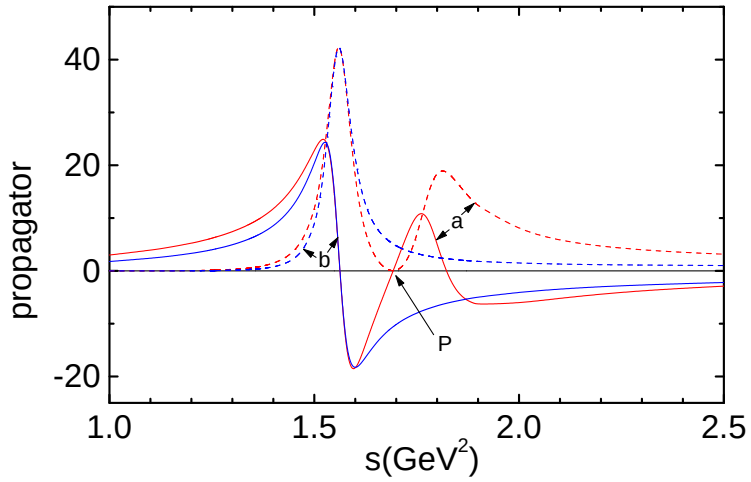

FIG. 14: Real (continuous line) and imaginary (dashed line) components of the two-resonance propagator (red curves a), given by eq.(B10), compared with the case of a single resonance propagator (blue curves b).

the P-wave components of these contributions are given by

$$\mathcal{K}_L^C = \frac{1}{2F^2}\,\boldsymbol{q}^2\,, \tag{C2}$$

$$\mathcal{K}_L^S = -\,\frac{4}{F^4}\left\{\frac{2\tilde{c}_d^{\,2}\,\boldsymbol{q}^2}{3} + \left[\tilde{c}_d\,m_0^2 - 2(\tilde{c}_d - \tilde{c}_m)M_\pi^2\right]\left[\tilde{c}_d m_0^2 - 2(\tilde{c}_d - \tilde{c}_m)M_K^2\right]\,I_P^t(\boldsymbol{q}^2; m_0^2)\right\}$$

$$+\frac{1}{3F^4}\left\{\frac{2c_d^2\,\boldsymbol{q}^2}{3}+\left[c_d\,m_8^2-2(c_d-c_m)M_\pi^2\right]\left[c_d\,m_8^2-2(c_d-c_m)M_K^2\right]\,I_P^t(\boldsymbol{q}^2;m_8^2)\right\}$$

$$+\frac{1}{2F^4}\left\{-\frac{2c_d^2\,\boldsymbol{q}^2}{3}+\left[c_d\,m_{K_0^*}^2-(c_d-c_m)\,(M_\pi^2+M_K^2)\right]^2\,I_P^u(\boldsymbol{q}^2;m_{K_0^*}^2)\right\}\,, \tag{C3}$$

$$\mathcal{K}_{L\rho}^V=-\left[\frac{G_V}{F^2}\right]^2\left\{\frac{2\,\boldsymbol{q}^2}{3}+m_\rho^2\,\left[2(s-M_\pi^2-M_K^2)+m_\rho^2\right]\,I_P^t(\boldsymbol{q}^2;m_\rho^2)\right\}\,, \tag{C4}$$

$$\mathcal{K}_{L\,K^*}^V=-\frac{1}{4}\,\left[\frac{G_V}{F^2}\right]^2\left\{-\frac{2\,\boldsymbol{q}^2}{3}+\left[m_{K^*}^4+2m_{K^*}^2(s-M_\pi^2-M_K^2)-(M_\pi^2-M_K^2)^2\right]\,I_P^u(\boldsymbol{q}^2;m_{K^*}^2)\right\}\,, \tag{C5}$$

$$I_P^t(\boldsymbol{q}^2;m^2)=\frac{1}{2\boldsymbol{q}^2}\,\left\{1-\left[\frac{m^2}{4\boldsymbol{q}^2}+\frac{1}{2}\right]\,\ln\left[1+\frac{4\boldsymbol{q}^2}{m^2}\right]\right\}\,, \tag{C6}$$

$$I_P^u(\boldsymbol{q}^2;m^2)=-\frac{1}{2\boldsymbol{q}^2}\,\left\{1+\left[\frac{m^2+s-2(M_\pi^2+M_K^2)}{4\boldsymbol{q}^2}-\frac{1}{2}\right]\ln\left[1-\frac{4\boldsymbol{q}^2}{m^2+s-2(M_\pi^2+M_K^2)}\right]\right\}\,, \tag{C7}$$

where $\boldsymbol{q}$ is the three-momentum in the center of mass, F, $\tilde{c}_{d,m}$, $c_{d,m}$ and G_V are coupling constants.

Appendix D: numerical input

The fit on P-wave $K\pi$ amplitude with isospin 1/2 gives $\chi^2/n.d.f.=2.13$ for the phase and $\chi^2/n.d.f.=5.16$ for the modulus. All values used in this work are expressed bellow.

• Masses extracted from PDG 2012[11] in GeV: $M_\pi=0.13957\,,\ M_K=0.493677\,,\ m_\rho=0.77549\,,\ m_{K_0^*}=1.4250$.

• Low-energy parameters in GeV: $F=0.10272$ [12], $G_V=0.0930/\sqrt{2}$ [10], $c_d=0.0320$ [10], $c_m=0.0420$[10], $\tilde{c}_{d,m}=c_{d,m}/\sqrt{3}$ [10], $m_0=m_8=0.9830$ [7].

• Parameters extracted from $K\pi$ scattering data[8]: $m_{K^*}=0.894$ GeV , $C=0.005127$.

• Fitted parameters with errors in $\mathcal{K}_H$ eq.(16): $m_a=17.80354\,(0.60089)$ GeV, $g_a^2=2.80157\,(0.51899)\times10^6$ GeV^{-2}, $h_a=1.18961\,(0.00918)$ GeV, $\lambda_a^2=4.13935\,(0.29267)\times10^3$ GeV^{-2}, $m_b=1.64987\,(0.03025)$ GeV , $m_c=2.12355\,(0.01283)$ GeV, $g_b^2=12.50453\,(0.58872)$ GeV^{-2}, $g_c^2=26.80905\,(1.3371)$ GeV^{-2}, $\xi=0.22492\,(0.00848)$, $h_b=0.8\,(0.02211)$ GeV, where

h is related to the heavy mass by

$$Q = \frac{\sqrt{s}}{2}\left(1 - \frac{h^2}{s}\right), \tag{D1}$$

which is an approximation of eq.(A4) when one of the masses is considerably greater than the other.

• Fitted parameters in eq.(18): $\alpha = 1.39198\,(0.01063)$, $\beta = 2.52707\,(0.09216)$, $\gamma = 4.27768\,(0.20357)$.

---

[1] J.A. Oller, Phys. Rev. **D71**, 054030 (2005); I. Caprini, Phys.Lett. **B638**, 468 (2006); J. Gasser, B. Kubis and A. Rusetsky Nucl.Phys. **B850**, 96 (2011); B. Kubis, PoS QNP2012, 027 (2012); B. Kubis, PoS ConfinementX, 240 (2012) ; C. Hanhart, [hep-ph/1311.6627].

[2] P. C. Magalhães, M. R. Robilotta, K. S. F. F. Guimarães, T. Frederico,W. S. de Paula, I. Bediaga, A. C. dos Reis, and C.M. Maekawa, G.R.S. Zarnauskas, Phys. Rev. D**84**, 094001 (2011); P. C. Magalhães, M. R. Robilotta, hep-ph/1307.8352; P. C. Magalhães, M. R. Robilotta, hep-ph/1312.2033.

[3] C.B. Lang, Nucl. Phys. B**93**, 415 (1975).

[4] J.A. Oller and E. Oset, Phys. Rev. D **60**, 074023 (1999); Nucl. Phys. A **620**, 465 (1997); A **652**, 407(E) (1999).

[5] K.P. Khemchandani, A. Martinez Torres, H. Nagahiro and A. Hosaka, Phys.Rev. **D88**, 114016 (2013);

[6] J.A. Oller, E. Oset and J.R. Pelaez, Phys.Rev. D**59**, 074001 (1999), Erratum-ibid. D**60**, 099906 (1999), Erratum-ibid. D75 (2007) 099903; A. Dobado, J.R. Pelaez, Phys.Rev. D**56**, 3057 (1997); Phys.Rev. D**47**, 4883 (1993).

[7] J. Gasser and H. Leutwyler, Nucl. Phys. B**250**, 465 (1985); Ann. Phys. **158**, 142 (1984).

[8] D. Aston et al., Nucl.Phys. B **296**, 493 (1988).

[9] S. Weinberg, Physica A **96**, 327 (1979).

[10] G. Ecker, J. Gasser, A. Pich and E. De Rafael, Nucl. Phys. B **321**, 311 (1989).

[11] J.Beringer, Phys.Rev. **D86**, 010001 (2012).

[12] M. Jamin, J.A. Oller and A. Pich, Nucl. Phys. B **587**, 331 (2000).